Journal of the Korean Physical Society, Vol. 77, No. 11, December 2020, pp. 1021∼1025

A-site Doping Effect of Multiferroic $BiFeO_3$ Ceramics

Taekyung Lim*
Department of Physics, Kyonggi University, Suwon 16227, Korea

Ok Sung Jeon,* Yunju La, Sang Yoon Park† and Young Joon Yoo‡
Advanced Institutes of Convergence Technology, Seoul National University, Suwon 16229, Korea

Keun-Hyeok Yang
Department of Architectural Engineering, Kyonggi University, Suwon 16227, Korea

(Received 30 September 2020; revised 22 October 2020; accepted 22 October 2020)

The structural, magnetic and ferroelectric properties of polycrystalline *A*-site (A = Ho, Pr and Ce of 10%) doped $BiFeO_3$, which were prepared by the solid-state and rapid sintering methods, have been investigated. The powder X-ray diffraction pattern reveals that all the samples show rhombohedral perovskite structure *R3c*. The Ho-doped $BiFeO_3$ shows that the magnetic property is slightly increased due to compressive lattice distortion and Ho^{3+} ion doping effect. For the Pr and Ce doped $BiFeO_3$, the remnant polarization and coercive field increased because Pr^{3+} and Ce^{3+} ions substitution suppressed oxygen vacancies.

Keywords: $BiFeO_3$, Multiferroics, Canted spin structure, Polarization-electric curve
DOI: 10.3938/jkps.77.1021

I. INTRODUCTION

In the information age, people have acquired more and more information, and thus, more information has been stored. According to the trend of the times, there is a need for a work to greatly improve the capacity of memory devices. In order to develop a large-scale memory device, an integrated circuit is used to increase data storage capacity. However, since the limit of capacity that can be improved through integrated circuits is clear, studies using new methods have been suggested.

As a method for maximizing the storage capacity of the device, studies on multiferroics have been actively conducted. The multiferroics refers to a material that has two or more properties at the same time, and generally refers to the case of having ferromagnetic and ferroelectric properties [1–4]. The ferromagnetic property is being divided into N- and S-poles like a magnet, and ferroelectric is a property that becomes polarized by being divided into positive (+) and negative (−) in molecule. By using the property of dividing into two states, a memory device can be made. For example, the case where the anode is on top is recognized as '1' and the case where the cathode is on top is recognized as '0' and information is stored. The multiferroics has many advantages as it can use both magnetic and electric fields because it can be adjusted with either a magnetic or electric field. In addition, not only $N-S$ pole alignment but also information storage according to the polarization state is possible, increasing storage efficiency and integration. The power consumed by generating the magnetic field in the existing memory and the resulting heat generation can be reduced, and thus the power consumption can be significantly reduced. Furthermore, if both ferromagnetic and ferroelectricity properties can be memory, signals that were previously stored only as 0 and 1 can be separated into 0, 1, 2, 3 and stored, which can increase the existing storage capacity to square scale [5–7].

Among the multiferroics, $BiFeO_3$ (BFO) has been the most researched material in the last 15 years, and has a phenomenon in which spin structure and electric polarization are combined, and based on this, research is underway to convert the device at room temperature [8–10]. BFO has the structure of rhombohedral perovskite ABO_3 at room temperature. The magnetic properties of BFO are antiferromagnetic Neel temperature at 643 K, and the ferroelectric properties have ferroelectric Curie temperature at 1103 K. The magnetic structure of BFO shows G-type AFM order modulated by a cycloid spin structure (∼62 nm) below the Néel temperature where antisymmetric Dzyaloshinskii−Moriya (D−M) exchange interactions. These interactions are caused by the combined action of Fe−O−Fe super-exchange and spin−orbit interactions, produce a weak ferromagnetic

*These authors contributed equally to this work.
†E-mail: yoonpark77@snu.ac.kr
‡E-mail: youngjoonyoo@snu.ac.kr

moment (∼0.02 μB/Fe) due to a canting of the Fe sublattice [11,12]. On the other hand, the stereo chemical activity of Bi $6s^2$ lone-pair electrons, hybridized with both the empty $6p^0$ orbitals of Bi^{3+} ion and the $2p^6$ states of O^{2-} ion, is responsible for noncentro-symmetric ferroelectric order along the [111] direction of the cubic perovskite-like lattice [13–15].

Contrary to known wide application possibilities, BFO has a disadvantage in that ferroelectric properties are degraded by a large leakage current due to space-charge defects such as oxygen defects. Another disadvantage is that the magnetic properties are very weak due to the disappearance of net magnetization due to the cycloid spin structure having a period of 62 nm [16]. In order to enhance ferroelectric properties, tetravalent ions were substituted for *A*-site or *B*-site or oxygen deficiency was suppressed [17–19]. In order to reinforce the magnetic properties, an attempt was made to break the magnetic cycloid spin structure like nanoparticle manufacturing [20,21], and by replacing the 3d transition metal instead of Fe in the *B*-site, a change in magnetic interaction was improved properties [22–25]. As a study to improve both properties, a method of simultaneously replacing *A*-site and *B*-site was also proposed [26–29].

In this study, we report a study in which various materials were substituted for *A*-site in BFO powder. Ho, Pr, and Ce were substituted at the *A*-site, and structural characteristics, magnetic characteristics, and ferroelectric characteristics were analyzed through X-ray diffraction measurement. In consideration of the applicability to memory devices, all measurements were performed at room temperature, and magnetic and ferroelectric hysteresis loops were carefully analyzed to understand the basic characteristics of the storage device.

II. EXPERIMENTAL SETUP

Polycrystalline BFO, $Bi_{0.9}Ho_{0.1}FeO_3$ (BFO-Ho: Ho-doped sample), $Bi_{0.9}Pr_{0.1}FeO_3$ (BFO-Pr: Pr-doped sample), and $Bi_{0.9}Ce_{0.1}FeO_3$ (BFO-Ce: Ce-doped sample), were prepared by the conventional solid-state reaction method of rapid sintering process. The stoichiometric amounts of high-purity (99.99%) Bi_2O_3, Fe_2O_3, Ho_2O_3, Pr_2O_3, and Ce_2O_3 powders were thoroughly mixed, and subsequently calcined in the air at 600 °C for 24h with an intermediate grinding for the homogenization. And then the calcined mixture was cold pressed into pellets, and sintered at 800 °C in air for 1h. All the samples were slowly cooled to RT in a furnace for the sufficient oxidation. The crystal structures of samples were studied by powder X-ray diffraction (XRD: Rigaku Miniflex diffractometer) using Cu-Kα radiation. The magnetic property measurements were performed with a vibrating-sample magnetometer (VSM: Lakeshore 730). The ferroelectric hysteresis loop was obtained using RT66B Test System (Radiant Technologies, Inc.).

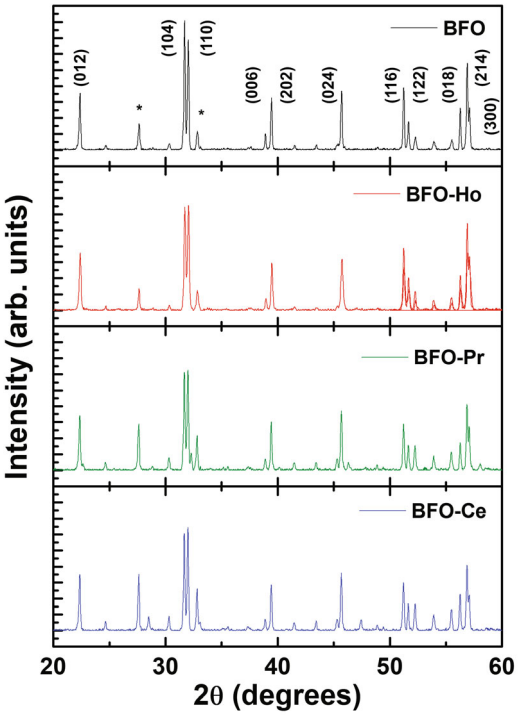

Fig. 1. Powder XRD patterns of BFO, BFO-Ho, BFO-Pr and BFO-Ce.

Table 1. The positions of main XRD peak around 32 degrees for all samples.

	BFO	BFO-Ho	BFO-Pr	BFO-Ce
Peak of (104)	31.71°	31.73°	31.69°	31.67°
Peak of (110)	32.03°	32.06°	32.00°	32.00°

III. RESULTS AND DISCUSSION

Figure 1 shows the powder-XRD patterns at room temperature of BFO, BFO-Ho, BFO-Pr and BFO-Ce samples. It is observed from the XRD results that all prepared samples are polycrystalline and can be indexed according to the rhombohedral perovskite structure with space group *R3c*. The XRD patterns show that the small impurity peaks (indicated by stars) are observed around $2\theta = 30°$, corresponding to $Bi_{12}(Bi_{0.5}Fe_{0.5})O_{19.5}$, while no other secondary phases are detected in all samples. Table 1 is information on the main XRD peaks of (104) and (110) around 32 degrees. The diffraction peaks of BFO-Ho sample shift slightly to higher angle as compared with that of the pristine sample (BFO), indicating a compressive lattice distortion associated with polarization switching [30]. This indicates changes of the lattice parameters due to the fact that the ionic radius of Ho^{3+} (0.0901 nm) is smaller than that of Bi^{3+} (0.1030 nm). For BFO-Pr and BFO-Ce, the diffraction peaks shift to smaller angle. These results indicated that the lattice

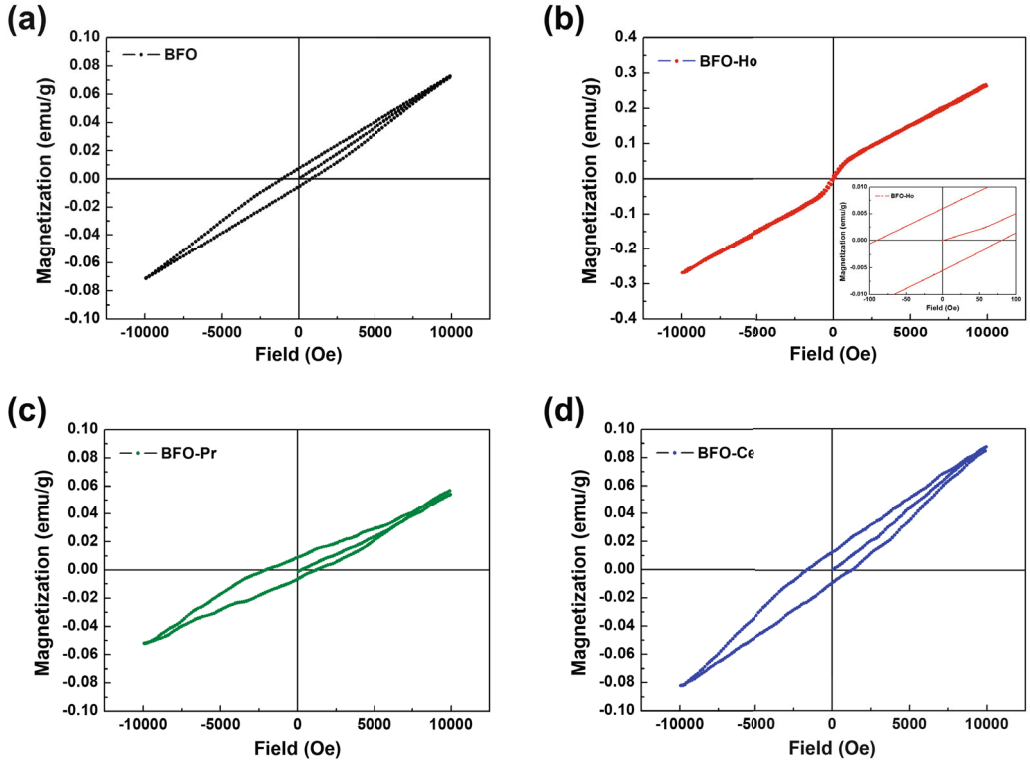

Fig. 2. Magnetic-field dependence of the magnetization at room temperature for (a) BFO, (b) BFO-Ho, (c) BFO-Pr and (d) BFO-Ce.

Table 2. The remnant magnetization (M_r) and coercive field (H_C) in magnetic hysteresis curve.

	BFO	BFO-Ho	BFO-Pr	BFO-Ce
M_r (emu/g)	0.006	0.006	0.008	0.011
H_C (Oe)	800	80	2070	1670

constant is slightly increased for BFO-Pr and BFO-Ce. The ionic radii of Pr^{3+} (0.099 nm) and Ce^{3+} (0.101 nm) are 2∼4% smaller than that of Bi^{3+}. The lattice constant of for BFO-Pr and BFO-Ce is expected to increase slightly because the material with almost similar ion radius is doped. Consequently, the XRD patterns reveal that all *A*-site doped samples do not affect the crystal structure of parent BFO, except for a slight variation of the lattice constant.

Figure 2 presents the magnetic hysteresis ($M-H$) loops for all the samples. Table 2 is remnant magnetization and coercive field of all samples in magnetic hysteresis curve. It is clearly observed that BFO exhibits nearly linear $M-H$ loop with small values of the remnant magnetization of 0.006 emu/g and the coercive field of 800 Oe, suggesting antiferromagnetic behavior with weak-ferromagnetic to show the unsaturated magnetization and the slim hysteresis loop. Compared to the pristine BFO, the maximum magnetization value has enhanced significantly in BFO-Ho sample, as shown in Fig. 2(b). The $M-H$ curve exhibits a slim *S*-shaped hysteresis loop without saturation, which also turns out to be weak ferromagnetic behavior. Another noteworthy aspect in Fig. 2(b) is that the reduction of $M-H$ loop area indicates the decreased ferromagnetic component, and that the linear increase of magnetization at higher field is observed. When *Rare Earth* ions are substituted Bi^{3+} in BFO, the magnetization value is affected by the magnetic moments of the ions. These features can be expected for in terms of Ho^{3+} ions (10.4 μ_B) contribution, leading to the magnetic moments aligned along the external magnetic field. It was revealed that the Ho dopant favors the magnetic exchange interactions in BFO ceramic. The $M-H$ curves for BFO-Pr and BFO-Ce reflect the slim hysteresis loop (Figs. 2(c) and 2(d)). The remnant magnetization increases slightly by the doping of Pr and Ce. The value of coercive field for BFO-Pr and BFO-Ce also increases, which are 2070 Oe and 1670 Oe, respectively. These results indicated that the magnetic properties of BFO-Pr and BFO-Ce are similar to the weak ferromagnetic behavior due to spin canting. Considering the application to the device, BFO-Ce seems useful because the value of remnant magnetization is relatively large, but the coercive field that is more than twice as large as BFO, acts as a disadvantage. On the other hand, BFO-Ho has the remnant magnetization similar to that of the pristine BFO, but it can be used as the device because it can make the magnetization value 0 with small magnetic coercive field (= 80 Oe).

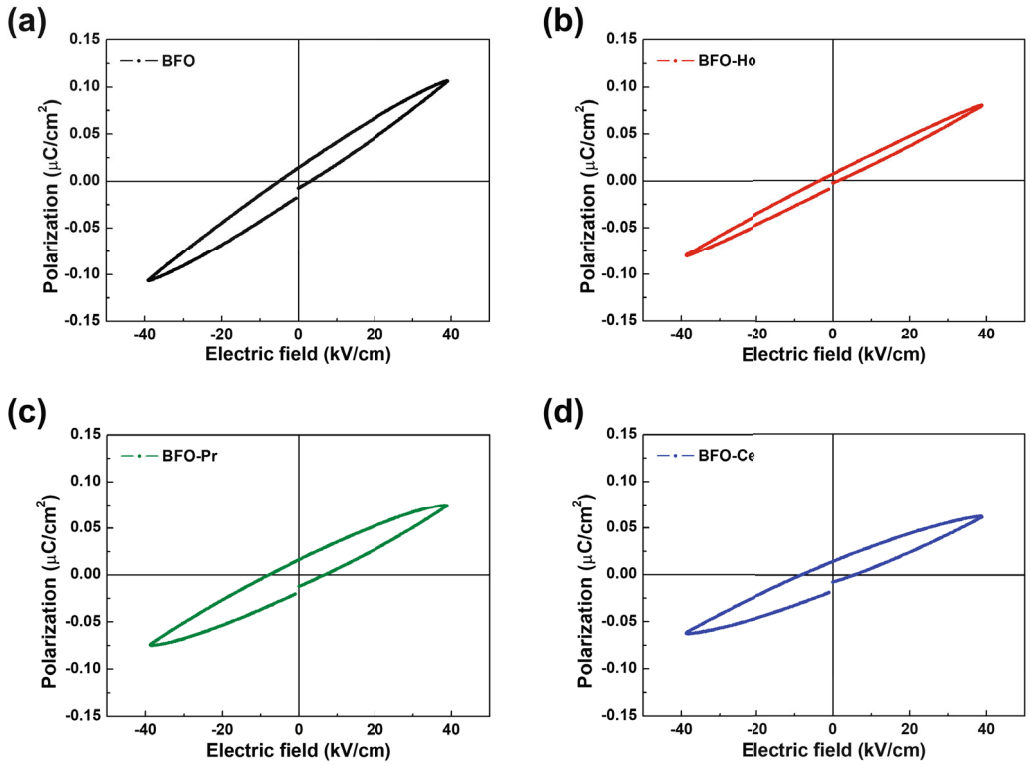

Fig. 3. $P-E$ hysteresis loop of (a) BFO, (b) BFO-Ho, (c) BFO-Pr and (d) BFO-Ce.

Table 3. The double remnant polarization and coercive field in $P-E$ curves.

	BFO	BFO-Ho	BFO-Pr	BFO-Ce
$2P_r$ ($\mu C/cm^2$)	0.028	0.014	0.032	0.030
E_C (kV/cm)	5.15	3.07	8.30	8.30

To investigate the ferroelectric properties of A-site doped BFO, the polarization hysteresis loop for all samples was measured under electric field range of -40 to 40 kV/cm. Figure 3 presents the ferroelectric hysteresis ($P-E$) loops of all the samples at 100 Hz and room temperature. Table 3 is double remnant polarization and coercive field of all samples in $P-E$ curves. The BFO shows an unsaturated lossy loop with small double remnant polarization ($2P_r$) of 0.028 $\mu C/cm^2$, revealing high conductivity due to the space charge defects [31]. For BFO-Ho, as shown in Fig. 2(b), the polarization hysteresis loop reflects a pinched hysteresis loop compare with case of BFO. The maximal polarization, remnant polarization (P_r), and coercive field (E_C) decreased with Ho-doping. It is seen that, for BFO-Pr and BFO-Ce, the $P-E$ loop with $2P_r$ (0.032 $\mu C/cm^2$ and 0.030 $\mu C/cm^2$, respectively) is similar to that of BFO in shape. The result of the slight increment of double remnant polarization and the unsaturated lossy loop. Another noteworthy aspect in Figs. 3(c) and 3(d) is that the hysteresis loop appears slightly saturated around 40 kV/cm in BFO-Pr and BFO-Ce. In addition, the two samples showed less gap in hysteresis than BFO. The ferroelectric property of the BFO originated from the displacements of Bi with respect to the FeO_6 cages along the (111) plane [32]. For BFO-Pr and BFO-Ce, the enhanced remnant polarization and coercive field might be attributed to the structure distortion because Pr- and Ce-ions are partially substituted for Bi^{3+}, thus resulting in the decreased oxygen vacancies by the stabilized oxygen octahedron [33]. BFO-Pr and BFO-Ce show the characteristics of being slightly saturated, but a large electric field is required to make the remnant polarization of 0. On the other hand, in the case of BFO-Ho, the maximum polarization is small, but the polarization can be transitioned with an electric field of 3.07 kV/cm.

IV. CONCLUSION

We prepared samples in which Ho, Pr, and Ce were substituted on the A-site of BFO, and the structural, magnetic, and ferroelectric properties of all samples were analyzed at room temperature. Based on structural characteristics analysis, it was found that compressive lattice distortion occurred in the case of Ho-substituted samples. In the case of BFO-Pr and BFO-Ce, the structural lattice constant was slightly increased. The magnetic-field dependence of the magnetization significantly increases in magnetization in the Ho doped BFO,

which is inferred to be due to compressive lattice distortion and magnetic moments of Ho ions. The remnant polarization and coercive field increased in the case of Pr and Ce doped BFO in $P-E$ curve measurement due to the fact that Pr^{3+} and Ce^{3+} ions are replaced with Bi ion sites and play a role of suppressing oxygen deficiency. Based on the results of this study, it was confirmed that magnetic properties can be slightly enhanced by inducing compressive lattice distortion through *A*-site substitution, and ferroelectric properties can be slightly increased by suppressing oxygen defects.

ACKNOWLEDGMENTS

This work was supported by the Korea Institute of Energy Technology Evaluation and Planning (KETEP) and the Ministry of Trade, Industry & Energy (MOTIE) of the Republic of Korea (No. 20181110200070).

REFERENCES

[1] W. Eerenstein, N. D. Mathur and J. F. Scott, Nature **442**, 759 (2006).
[2] Y. Tokura, J. Magn. Magn. Mater. **310**, 1145 (2007).
[3] D. I. Khomskii, Bull. Am. Phys. Soc. C **21**, 002 (2001).
[4] M. Fiebig *et al.*, Nature **419**, 818 (2002).
[5] M. Fiebig, J. Phys. D: Appl. Phys. **38**, R123 (2005).
[6] K. M. Song *et al.*, Phys. Rev. B **83**, 012404 (2011).
[7] S. Mori *et al.*, Phys. Rev. B **72**, 224434 (2005).
[8] X. Qi *et al.*, Appl. Phys. Lett. **86**, 062903 (2005).
[9] W. Eerenstein *et al.*, Science **307**, 1203 (2005).
[10] N. A. Spaldin and M. Fiebig, Science **309**, 391 (2005).
[11] J. M. Moreau, C. Michel, R. Gerson and W. J. James, J. Phys. Chem. Solids **32**, 1315 (1971).
[12] C. Michel *et al.*, Solid State Commun. **7**, 701 (1969).
[13] F. Kubel and H. Schmid, Acta Crystallogr. Sect. B **46**, 698 (1990).
[14] R. Seshadri and N. A. Hill, Chem. Mater. **13**, 2829 (2001).
[15] P. Ravindran, R. Vidya, A. Kjekshus and H. Fjellvag, Phys. Rev. B **74**, 224412 (2006).
[16] Y. F. Popov *et al.*, JETP Lett. **57**, 69 (1993).
[17] S. J. Kim *et al.*, J. Korean Phys. Soc. **56**, 439 (2010).
[18] F. Yan, M-O. Lai, L. Lu and T-J. Zhu, J. Phys. Chem. C **114**, 6994 (2010).
[19] F. Zhang *et al.*, Materials **11**, 2208 (2018).
[20] A. Bombik, B. Lesniewska, J. Mayer and A. W. Pacyna, J. Magn. Magn. Mater. **257**, 206 (2003).
[21] J. S. Zhou and J. B. Goodenough, Phys. Rev. B **77**, 132104 (2008).
[22] Y. J. Yoo *et al.*, J. Appl. Phys. **114**, 163902 (2013).
[23] J. S. Hwang *et al.*, J. Korean Phys. Soc. **69**, 282 (2016).
[24] T. Gholam*et al.*, Phys. Lett. A **381**, 2367 (2017).
[25] A. K. Sinha *et al.*, Results Phys. **13**, 102299 (2019).
[26] K. Chakrabarti *et al.*, Appl. Phys. Lett. **101**, 042401 (2012).
[27] A. Mukherjee *et al.*, Physica B **448**, 199 (2014).
[28] Y. J. Yoo *et al.*, J. Magn. Magn. Mater. **374**, 669 (2015).
[29] F. L. Wang *et al.*, J. Alloys Compd. **810**, 151941 (2019).
[30] H. Liu *et al.*, Phys. Rev. B **87**, 220101(R) (2013).
[31] V. R. Palkar, J. John and R. Pinto, Appl. Phys. Lett. **80**, 1628 (2002).
[32] J. Wang *et al.*, Science **299**, 1719 (2003).
[33] Z. Quan *et al.*, J. Appl. Phys. **104**, 084106 (2008).